Experimental and numerical investigation into the propagation of entropy waves

Andrea Giusti*, Nicholas A. Worth†, Epaminondas Mastorakos‡ and Ann P. Dowling§
University of Cambridge, CB2 1PZ Cambridge, UK

Entropy waves are an important source of indirect combustion noise and potentially contribute to the generation of thermoacoustic instabilities in gas-turbine combustors. Entropy fluctuations generated by unsteady combustion are known to disperse and diffuse as they convect towards the combustor exit. In this work the propagation of entropy waves is investigated by means of experiments in a newly developed entropy rig and numerical simulations based on the LES approach. Both experimental and numerical results demonstrate that the amplitude of entropy fluctuations decays as a function of wave parameters and propagation distance and scales well with a local Helmholtz number, He. A new theoretical model for the computation of the entropy transfer function suitable for inclusion in low-order models for combustion instabilities is proposed. Assessment against numerical and experimental results shows the capability of the model to give a proper representation of the decay of entropy waves in terms of both magnitude and phase of the entropy transfer function. Furthermore, by comparison with the LES results, it is shown that at low He the contribution of the differential convection to the decay of entropy waves is dominant whereas for high values of He the turbulent mixing and diffusion also become important.

---

* Research Associate, Department of Engineering, Trumpington Street. Member AIAA.
† Research Associate, Department of Engineering, Trumpington Street. Now, Associate Professor, Department of Energy and Process Engineering, Norwegian University of Science and Technology.
‡ Professor, Department of Engineering, Trumpington Street. Associate Fellow AIAA.
§ Professor, Department of Engineering, Trumpington Street. Fellow AIAA.

I. Introduction

Combustion noise and thermoacoustic instabilities are becoming very important issues in the design of gas-turbine combustors, especially when the lean-burn combustion technology is exploited [1]. Therefore, in recent years great attention has been devoted to the investigation of the phenomena related to noise generation and flame-acoustics interaction. As discussed in the early work of Marble and Candel [2], the presence of a non-uniform distribution of entropy in the flow, for example hot and cold spots generated by unsteady combustion and convected by the mean flow, could be an important source of indirect noise when it is accelerated as it is in the case of the choked nozzle located at the exit of a gas-turbine combustor. The acceleration of entropy waves through a nozzle also generates pressure waves that propagate upstream towards the flame possibly leading to thermoacoustic instabilities [3, 4]. The form of propagation of the entropy waves is based on convection but the amplitude of such waves can also be affected by diffusion and dispersion.

Entropy waves, typically generated in the flame region even if in some configurations additional contributions may also come from the dilution with cold flow [5], are convected to the combustor exit by a mean flow which is non-uniform over the combustor cross-section and subject to intense turbulent fluctuations which can contribute to the diffusion of entropy waves, especially when the wavelength of entropy fluctuations is small in comparison with the turbulent length scale [6, 7]. On the contrary, when the wavelength of entropy perturbations is long compared with the turbulent length scale, the turbulent mixing does not lead to any significant diffusion of such perturbations [8]. Non-uniformities in the mean flow profile cause different residence times of disturbances generated at different radial positions and, as discussed in [1, 7], this tends to reduce their cumulative effect and hence the strength of the induced acoustic wave, in a phenomenon usually referred to as shear dispersion. The importance of the effect of a mean velocity profile which varies across the section on the propagation of entropy waves was also recently pointed out by Morgans et al. [9] through a Direct Numerical Simulation (DNS) of a simplified turbulent channel flow between two parallel plates. The work by Morgans et al. [9] can be considered one of the first attempts to estimate the dispersion of entropy waves using Computational Fluid Dynamics (CFD). Neglecting the effect of heat addition due to combustion and assuming the flow to be incompressible (so that the temperature and entropy

fluctuations scale with one another), a Gaussian perturbation of the temperature was introduced at the inlet boundary and its propagation along the channel was analysed. It was found that the losses in entropy strength are mainly related to the differential convection due to a non-uniform mean flow across the section. A Gaussian model for the entropy transfer function (which gives a one-dimensional description of the relation between the entropy fluctuations at the outlet of the channel and the inlet perturbation) was also suggested and assessed against the numerical data in terms of magnitude, whereas no comparison between the phase predicted by the model and the numerical results was given. Some experiments to study phenomena related to entropy waves have also been performed (e.g. [10–13]), however the focus has usually been on the indirect noise generated by convection through a nozzle, whilst not much attention has been devoted to the characterization of the attenuation of entropy waves.

As far as low-order acoustic codes are concerned, although the importance of dispersion and diffusion of entropy waves has been pointed out by many authors [1, 7, 9, 14], attempts to model these effects are quite rare and such phenomena are usually not considered in simplified analytical and numerical models of entropy noise [2, 15, 16]. Furthermore, the few attempts to include the effect of entropy diffusion and dispersion (e.g. [7, 17]) are generally based on theoretical and heuristic arguments without any validation against experimental data.

In order to give more insight into the phenomena occurring during entropy wave propagation and to analyse the diffusion and dispersion of such waves, numerical simulations and experiments in a newly developed small-scale entropy rig have been performed. Furthermore, a new theoretical model for the computation of the entropy transfer function, suitable for low-order acoustic network codes, has been introduced and assessed against the data obtained in the experiment and numerical simulations. Experimental and numerical results, as well as the new low-order model for the attenuation of entropy waves, are presented and discussed in this paper.

The paper is structured as follows. In Section II the small-scale entropy rig is described and experimental results are discussed. Section III is devoted to the numerical investigation. The numerical method and the computational setup are first presented followed by a validation of the method and comparisons with experimental results. In Section IV the new theoretical model for

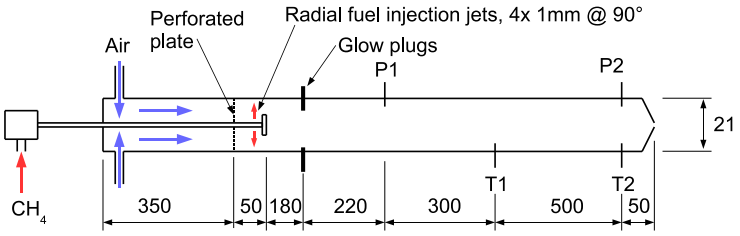

Fig. 1 Schematic of the entropy rig

Table 1 Ranges of U_b and Re_D investigated in the experiment.

	U_b (m/s)	Re_D
$d_{noz} = 2.5$ mm	3.4-4.1	2200-3100
$d_{noz} = 3.5$ mm	6.8-7.8	6600-7700

the entropy transfer function is described. Validation is performed against data collected in the experimental and numerical investigations with focus on both the magnitude and the phase of the entropy transfer function. Comparisons with other models available in literature [7, 9] are also discussed. Conclusions and recommendations for future research close the paper.

II. Experiments

In this section, the small-scale entropy rig is presented, followed by a description of the results obtained in the experimental investigation. Comparisons with numerical results will be discussed in Section III C with the main aim of giving useful information for the development of low-order models for the entropy wave attenuation.

A. Small-scale entropy rig

A schematic of the entropy rig illustrating the key features and dimensions is shown in Fig. 1. The rig consists of an insulated long stainless steel pipe with an inner diameter $D = 21$ mm and total length $L_T = 1650$ mm. A perforated plate was located at $z_p = 350$ mm for both flow conditioning and acoustic damping. Air entered the rig upstream via two opposing air jets ports. A fuel supply pipe of outer diameter 6 mm was positioned concentrically, extending to a distance of $z = 400$ mm. The fuel, methane (CH_4) was used in all these experiments, was injected through four crossflow jets

of diameter $d_j = 1$ mm spaced at 90° increments around the fuel pipe. A bluff body of diameter $d_{bb} = 12$ mm was located 10 mm downstream of the fuel injection point to enhance mixing. Reactant flow rates were controlled using rotameters with ranges of 12 SLPM and 200 SLPM for fuel and air respectively, to maintain a global equivalence ratio of $\phi = 0.35$. The reactant mixture was ignited by two 24 V glow plugs, which protrude 3 mm into the flow at an axial location z=580 mm. The experiment was run until thermal equilibrium had been reached before data acquisition commenced. To generate entropy fluctuations, a fast response valve, controlled by a TGP110 pulse generator, was connected into the fuel line 670 mm upstream of the injection location. Pulsing close to the natural frequency of the system at 10.7 Hz permitted the generation of large amplitude entropy waves. A pulse width of 27 ms was selected to achieve reliable ignition performance. The combustor was operated with a nozzle diameter d_{noz}=2.5 mm or d_{noz}=3.5 mm at exit. It should be noted here that the use of a choked nozzle is not mandatory to analyse the attenuation of entropy waves, however operating at a choked condition allows the effect of entropy wave diffusion and dispersion to be assessed using an engine relevant boundary condition. To vary the nozzle mass flow, the upstream pressure was varied from approximately 190 to 230 kPa, resulting in different flow bulk velocities U_b. The ranges of U_b and the respective Reynolds numbers (based on the rig diameter D), Re_D, investigated with the two nozzle configurations are given in Table 1.

Two Kulite XCS-093 pressure transducers (sensitivity: 5.882 $\times 10^{-4}$ mV/Pa, range: 1.7 atm, accuracy: $\pm$0.15% full scale) were positioned at axial locations $z = 800$ mm and $z = 1600$ mm in order to capture the oscillating pressure response. The transducers were water cooled and flush mounted inside an acoustically semi-infinite stand off line, 270 mm from the combustor wall. The pressure signals were amplified and filtered before being digitised using a National Instruments 16 bit PCI6353 card. Two K-type bare wire thermocouples with a wire diameter of $d_w = 25$ μm were positioned along the combustor centreline at axial positions $T1 = 1100$ mm and $T2 = 1600$ mm to record unsteady temperature fluctuations. The signals were recorded using an SCXI-1328 block and SCXI-1000 module. Time series were acquired at 10 kHz with sample lengths of 30 s.

Temperature and pressure signals were analysed spectrally using the Fast Fourier Transform in order to determine their frequency centred complex amplitude. The thermocouple time constant,

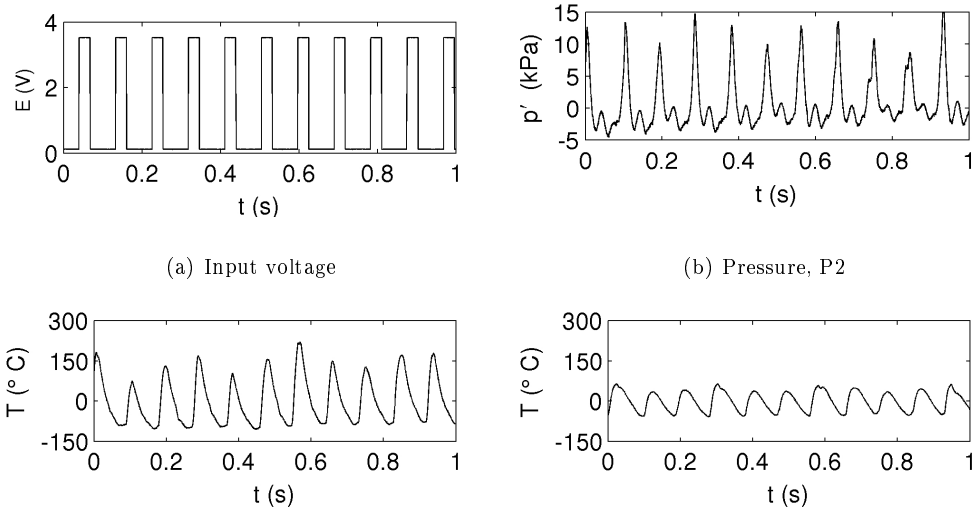

(a) Input voltage

(b) Pressure, P2

(c) Temperature, T1

(d) Temperature, T2

Fig. 2 Time series of fluctuating pressure, fluctuating temperature at two axial locations and signal generator input voltage for $d_{noz} = 2.5$ mm case. The bulk flow velocity is $U_b = 3.8$ m/s.

τ_c, was modelled using the approach of [18] as $\tau_c = \rho_w d_w C_w / 4h_w$, where ρ_w, C_w and h_w are the wire density, specific heat capacity and heat transfer coefficient respectively. The empirical correlation derived by McAdams [19] was used to estimate h_w, from $Nu = [0.35 + 0.56Re^{0.52}]Pr^{0.3}$, resulting in a time constant of approximately 40 ms, and a cut-off frequency of 25 Hz. This time constant was used to compensate for the attenuation and time lag associated with the thermal inertia at higher frequencies, and was implemented in the spectral domain through a transfer function [20], $H = 1/(1 - if\tau_c)$. An assessment of the response determined that frequencies below 80 Hz were sufficient in terms of their signal to noise ratio.

B. Experimental results

Figure 2 shows times series of the input signal voltage controlling the fuel supply, E (high voltages indicate the valve opening times), fluctuating pressure, and temperature at two axial locations. Once the valve is opened, fuel is injected into the airflow and convected downstream. The delay of approximately 42.5 ms between valve opening and the large pressure fluctuation shown in Fig. 2(b) corresponds to the distance between the fuel injection jet location, and glow plug location where

the fuel is ignited. The magnitude of the pressure response during ignition is considerable due to the flow confinement.

Figures 2(c) and 2(d) show temperature time series at the two axial locations, T1 and T2. Again, the temperature response at these locations lags the pressure fluctuation by approximately 0.115 s and 0.12 s respectively, corresponding again to the convection time of the hot combustion products. The magnitude of response at T1 is significantly larger than the response at T2, which is expected to arise from the mixing of hot products with surrounding fluid and phenomena related to the convection of the hot spots, resulting in the dispersion of the temperature and therefore of the entropy fluctuations. It is important to note that the level of entropy fluctuations is determined by both the pressure and temperature oscillations, however in the current setup the contribution due to the temperature is dominant and therefore in the following discussion the entropy fluctuations will be related to temperature oscillations only.

While the system is capable of operating reliably without misfiring (defined as the failure to ignite an injected pulse of fuel), the variation in the amplitude of both pressure and temperature fluctuations at location T1 are representative of variations in the ignition performance, due to the non-premixed nature of the system. Each successive pulse generates a spatially unique mixture of fuel and air, which is ignited and burned over a different time scale, resulting in the observed variations in the peak temperature and pressures. The amplitude of these two metrics are seen to vary by up to 65%, demonstrating considerable variation between successive ignition events. While the variation between successive temperature fluctuations reduces downstream at location T2, these should still be considered significant (peak to peak variations of $\approx$40%). This reduction is expected as a result of the additional mixing during the convection of hot products downstream, which further contributes to the decay of entropy fluctuations.

Figure 3 shows spectra of the control valve input signal, pressure and both the original and compensated temperature fluctuations at the first axial location (T1), whereas Fig. 4 summarizes the location of the peaks in the original and compensated temperature spectra at the two axial locations (symbols represent the magnitude at the forcing frequency and the lowest 5 harmonics). As demonstrated in Fig. 3(a), the use of a square wave input signal results in the generation of a large

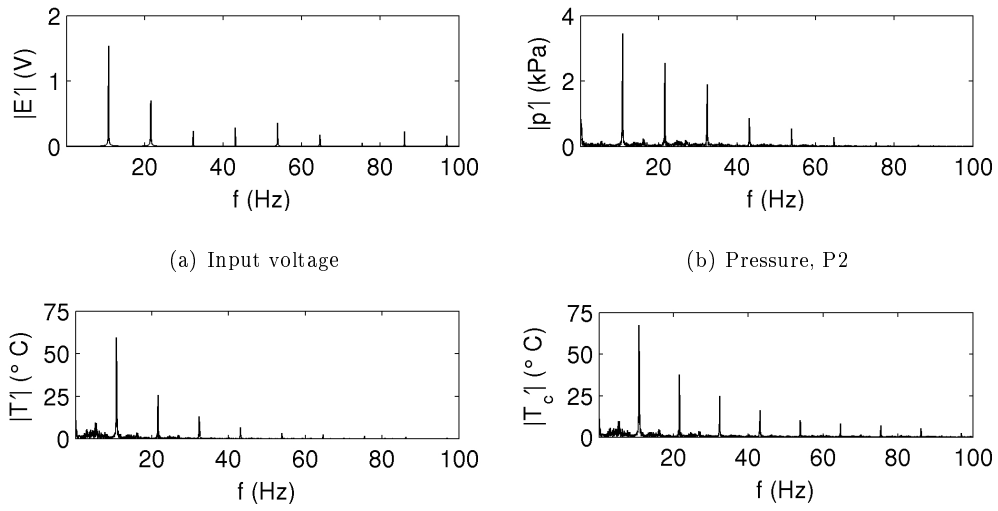

(a) Input voltage

(b) Pressure, P2

(c) Temperature, T1

(d) Compensated temperature, T1

Fig. 3 Pressure, original and compensated temperature, and signal generator input voltage spectra for $d_{noz} = 2.5$ mm case. The bulk flow velocity is $U_b = 3.8$ m/s.

number of harmonics, which decrease in amplitude with increasing frequency. Despite differences in their time series, the pressure and temperature response (shown in Fig. 3(b) and Fig. 3(c)) are also observed to contain significant energy in a range of harmonics, with the amplitude of fluctuations again shown to be inversely proportional to frequency. The simultaneous generation of a range of frequencies permits an investigation into the relative rate of decay of entropy waves. Typical values of the ratio between the fluctuation and the mean value of the temperature are in the range 0.01-0.10, where the highest values are reached for the fluctuations at the forcing frequency whereas the smallest ones are obtained for the higher harmonics.

It is also of interest to compare Fig. 4(a) and Fig. 4(b) to examine the effect of applying the thermocouple temperature compensation transfer function, H. The measured response of the temperature is observed to roll-off rapidly, with a very low amplitude response to even moderate frequencies ($f > 50$ Hz). In comparison, the use of the compensation transfer function, H, significantly increases the amplitude of response, and reduces spectral roll-off. The compensated temperature response is observed to more closely match the pressure response at high frequencies, suggesting that compensation is appropriate.

As expected from the time series plotted in Fig. 2, the amplitude of the response is larger at

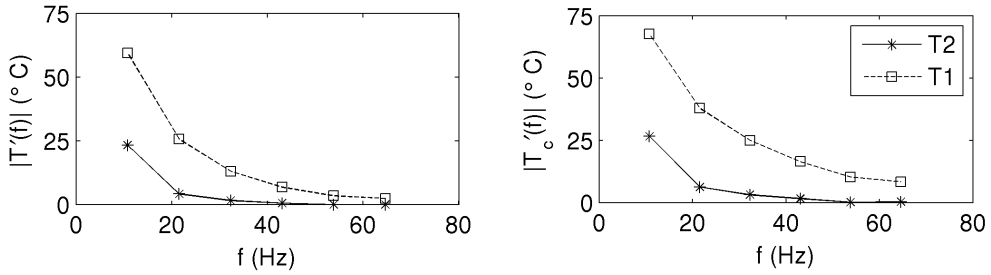

(a) Original response

(b) Compensated response

Fig. 4 Original and compensated temperature response at two axial positions for the first 6 harmonics ($d_{noz} = 2.5$ mm case). The bulk flow velocity is $U_b = 3.8$ m/s

the first axial position, and decreases significantly with axial distance. The response amplitude is also observed to monotonically decrease with increasing frequency. The decrease in amplitude at both locations T1 and T2 may be explained as the result of the unsteady injection and ignition of fuel, with the response likened to that of a square wave. The amplitude of the temperature response at location T2, is shown to decrease more rapidly with increasing frequency than that at location T1, suggesting that the attenuation of entropy waves increases with frequency. This point will be discussed further in Section III C where a measure of the decay of entropy fluctuations as a function of frequency is given.

It is also interesting to give an estimation of the level of entropy starting from temperature and pressure measurements. Figure 5 shows the time series and the spectra at T1 and T2 of the entropy estimated from temperature and pressure measurements using NASA polynomials and perfect gas relations and by assuming pure air composition (this can be considered a good approximation considering the low value of the global equivalence ratio). The effect of the pressure oscillations on the entropy level at the location T2 is also highlighted. It is possible to note that the entropy follows the same trend observed for the temperature and therefore, as already observed, all the previous considerations apply equally to both temperature and entropy. It is important to point out that the assessment of entropy fluctuations from single point measurements is challenging and in the present work the information coming from the experiment will primarily be used qualitatively even if, as shown in the following sections, also the quantitative information can be useful to assess the reliability of the numerical approach used to simulate the propagation of entropy waves.

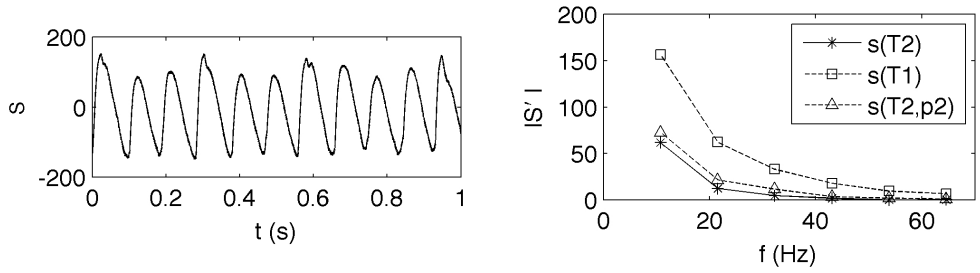

(a) Time series at T2.

(b) Entropy spectra.

Fig. 5 Estimated entropy time series at location T2 and spectra at two axial positions for the first 6 harmonics ($d_{noz} = 2.5$ mm case). The bulk flow velocity is $U_b = 3.8$ m/s

III. Numerical investigation using CFD

In order to better understand the phenomena affecting the decay of entropy fluctuations and generate data useful for the development of models for low-order network codes, CFD simulations of entropy wave propagation in a straight duct have been performed using a compressible Navier-Stokes equation solver developed in the OpenFOAM [21] (version 2.2) framework. The solver is based on a second-order accurate pressure-based formulation exploiting the PISO algorithm [22] for the solution of the pressure-velocity coupling. The energy equation was solved in terms of sensible enthalpy. The thermophysical properties of the fluid (assumed to be pure air) were computed using NASA polynomials whereas the Sutherland's law was used for the computation of transport properties (such as the molecular viscosity). The values of entropy used for the post-processing of entropy waves were directly extracted from the thermodynamic library as a function of both pressure and temperature.

A. Numerical modelling

Numerical simulations were performed using the Large Eddy Simulation (LES) approach. The computational domain consists of a circular duct with the same diameter of the experimental rig and an axial length $L = 0.5$ m, and it represents the part of the rig downstream of the ignition location. Figure 6 shows a schematic of the geometry together with the location of the different boundaries. The recycling and rescaling method [23] was used for the velocity at the inlet boundary, in order to reproduce a fully developed flow. The mapping plane was placed close to the exit of the

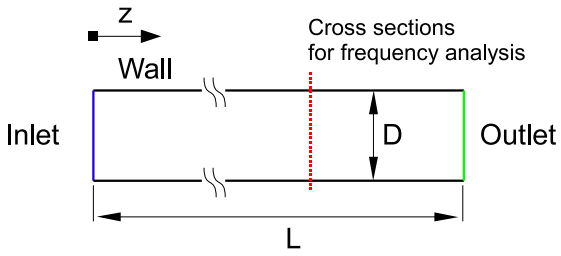

Fig. 6 Schematic of the cases investigated by CFD.

duct ($z/L = 0.99$) and the rescaling was performed by assigning the bulk velocity, U_b, of the flow. A non-reflecting condition, based on the advective concept [24] with linear relaxation, was used for pressure at the outlet allowing us to avoid the generation/reflection of acoustic waves at the exit of the domain. It should be noted that here the interest is only in the propagation of entropy waves and without pressure oscillations the entropy fluctuations can be related to temperature fluctuations only (the pressure oscillations due to compressibility effects give a negligible contribution to the level of entropy fluctuations and therefore in the following the observations made for the temperature also apply to the entropy). Entropy fluctuations were introduced at the inlet boundary by assigning a sinusoidal fluctuating temperature at a given frequency f and with a peak-to-peak amplitude equal to the 10% of the mean value: $T_{in}(t) = T_{mean}[1 + \alpha \sin(2\pi f t)]$ with $T_{mean} = 500$ K and $\alpha = 0.05$. At every time step the temperature is uniform at the inlet section. It should be noted that this assumption is probably not entirely representative of the experimental flow where the temperature profile depends on the ignition and mixing behaviour and changes with time. However, the use of this well-defined inlet condition will be useful in the derivation of low-order models (see Section IV A). Similar considerations also apply to the level of fluctuations and, even if in some of the experimental conditions higher fluctuations were observed, the amplitude chosen in the simulation allows us to obtain results relevant for the validation and assessment of low-order models based on small perturbations. No-slip adiabatic conditions were used for the wall of the duct.

The domain was discretised by means of a hexahedral mesh of about 4.5 million cells with a grid size in the axial direction equal to $\Delta z \sim 0.8$ mm, ensuring $\Delta z^+ < 50$ and at least 60 cells per wavelength of the entropy fluctuation (i.e. U_b/f) in all the investigated conditions. Refinement

Table 2 Investigated cases.

	f=50 Hz	f=100 Hz	f=200 Hz	Re_D
$U_b = 5.0$ m/s		•		2700
$U_b = 10.0$ m/s	•	•	•	5400
$U_b = 20.0$ m/s		•	•	10800

along the radial direction was adopted in the near wall region in order to have a y^+ of the first cell smaller than 1.0 and at least 3 cells in the viscous sublayer. The mesh spacing in the azimuthal direction satisfied $R\Delta\theta^+ < 25$ in all the cases. A sensitivity analysis to the grid size was also performed reducing Δz down to approximately 0.25 mm. Some significant variations appeared only in the cases characterized by a small wavelength of the entropy fluctuation with a maximum absolute deviation of the magnitude of the entropy transfer function (see in the following for the definition) of about 0.02. The constant Smagorinsky model was used for the sub-grid stress tensor together with van Driest damping [25, 26] to get the correct near-wall asymptotic behaviour of the sub-grid stresses. Second order accurate schemes were used for spatial discretization whereas the Crank Nicolson scheme was used for time derivatives.

Several simulations were performed varying the forcing frequency and the bulk velocity of the flow. Table 2 gives a summary of the cases investigated in this work. Computations were carried out at atmospheric pressure resulting in the same range of Reynolds numbers of the cases investigated in the experiment. Results will be presented in terms of 2D maps in the stream-wise section and frequency analysis at selected locations along the axis. In particular, with the perspective of exploiting results in low-order acoustic network codes, usually based on a one-dimensional formulation, frequency analysis will be applied to the time evolution of cross-section averaged values at several locations along the axis (mass-weighted averages have been used). A time step equal to 0.01 ms was used in all the simulations ensuring a Courant number lower than unity and a proper frequency range for frequency analysis. A fully developed flow solution, obtained without imposing the temperature fluctuation at the inlet boundary, was used as initial value in each simulation. Time averages (for the computation of local statistics in terms of mean value and variance of each

quantity) were initialized after two flow-through times and the total simulated time was chosen in order to have a proper frequency resolution and converged statistics.

B. Validation

Before analysing the entropy wave propagation, the capability of the adopted method to reproduce a fully developed flow throughout the duct was assessed by comparing results of a simulation without fluctuating temperature with data published in [27] for a fully developed turbulent pipe flow at Re=5400. Mean flow statistics presented in the following were obtained by performing an average over 10 flow-through times. A fully developed flow was established along the whole pipe with averaged profiles which do not change with the axial location. The instantaneous velocity field in a stream-wise cross section is shown in Fig. 7 where it is possible to appreciate the development of the turbulent structures. Figure 8 shows comparisons between the mean axial velocity profile from LES and experimental and DNS data from Eggels et al. [27] in both physical and wall units. The agreement is very good with the wall behaviour of the flow which appears well captured. Comparisons in terms of *rms* values for the three velocity components are shown in Fig. 9 (the *rms* values from the LES are based only on the resolved scales without including the sub-grid scale contribution). The agreement with the experimental measurements is good and follows the same trend observed by Eggels et al. [27] for DNS results (not reproduced here, please see the reference). Overall, the results are satisfactory and demonstrate the capability of the present numerical method to properly capture both the mean velocity profile and the turbulent fluctuations which, as will be discussed in the following, have an important role in the attenuation of entropy waves.

The numerical diffusion of the code was also assessed by simulating the entropy wave convection in a uniform flow. The numerical diffusion was evaluated in terms of decay of the amplitude of the entropy fluctuation at the exit of the duct resulting in a maximum value of the attenuation (found in the case characterized by the shortest wavelength of the entropy fluctuation, i.e. $f = 200$ Hz and $U_b = 10.0$ m/s) of about 7%. Smaller errors are present at the locations closer to the inlet of the duct and in the cases characterized by a longer wavelength of the entropy fluctuations. Overall, this level of error can be considered acceptable for the analysis performed here and confirms that both

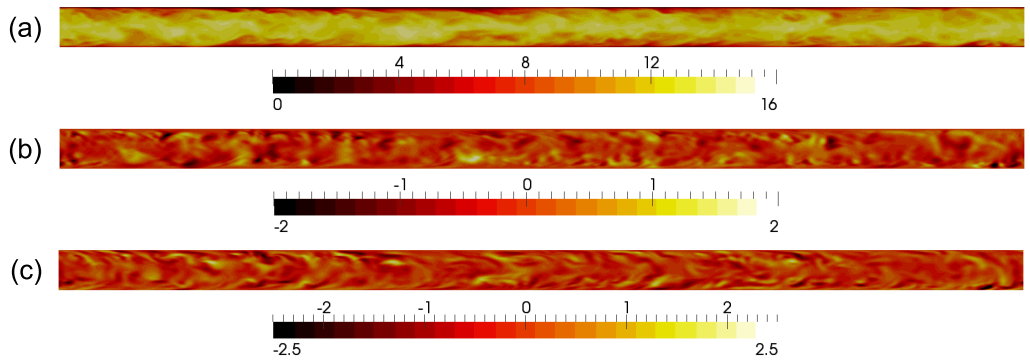

Fig. 7 Instantaneous velocity (m/s) for a fully developed pipe flow at Re=5400: (a) axial component, (b) radial component, (c) tangential component.

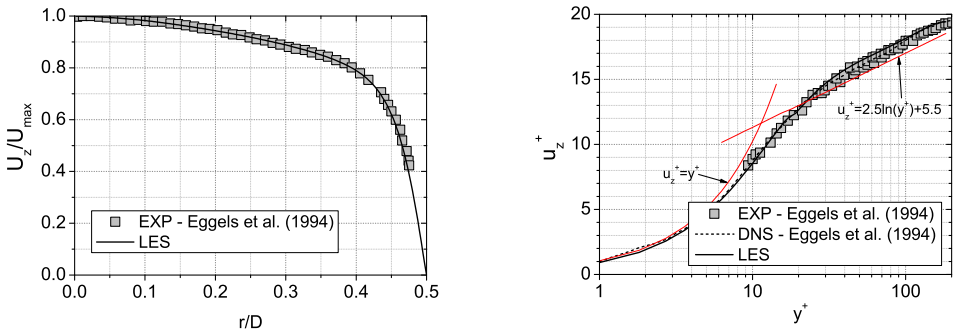

Fig. 8 Mean axial velocity for a fully developed pipe flow at Re=5400: comparison between present results and data published in [27].

the mesh and the numerical methods used in this work are suitable for the present investigation.

C. Results and discussion

Figures 10 and 11 show the instantaneous temperature and axial velocity in the stream-wise cross section of cases with the same bulk velocity ($U_b = 10$ m/s) but different forcing frequencies. It is possible to note that the temperature oscillation imposed at the inlet boundary is distorted along the duct because of the non-uniform velocity across the radius. Results show that the amplitude of oscillations decays as the wave moves towards the outlet and the amount of decay increases with the frequency, consistent with experiments. This is also clearly shown in Fig. 12 where the variance of the entropy field (i.e. the variance of the time evolution of the entropy at each spatial location)

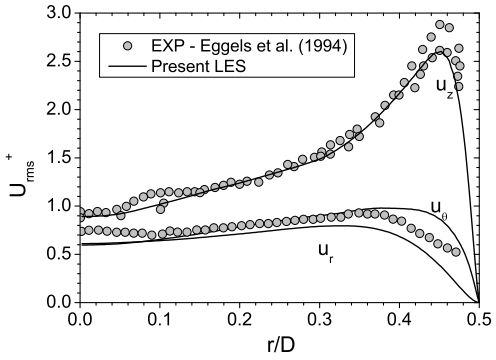

Fig. 9 Velocity fluctuations for a fully developed pipe flow at Re=5400: comparison between present results and data published in [27].

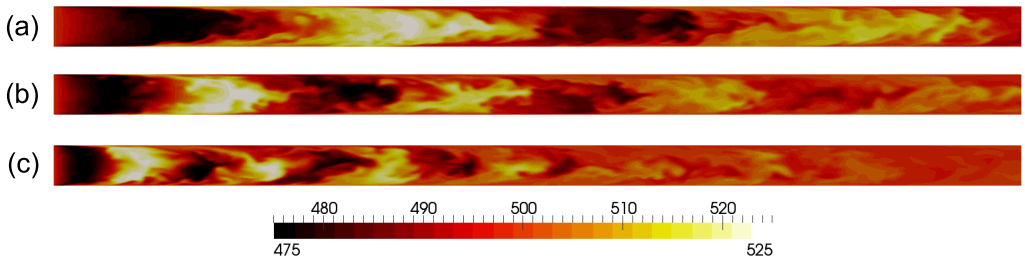

Fig. 10 Instantaneous temperature (K) at different frequencies ($U_b = 10.0$ m/s): (a) f=50 Hz, (b) f=100 Hz, (c) f=200 Hz.

is reported.

As also discussed in [7, 9], an important phenomenon that contributes to the decay of entropy fluctuations is the so called shear dispersion, caused by a non-uniform mean velocity profile over the cross-section. The non-uniform convection velocity across the radius determines time delays dependent on the radial position. Perturbations in the middle of the pipe, where the mean velocity is higher, move faster compared to the perturbations close to the walls and the hot and cold spots compenetrate each other losing the planar form imposed at the inlet boundary. This also generates gradients in the radial direction leading to radial diffusion which further contributes to the mixing between hot and cold spots. The combined effect of the differential time delay and radial diffusion is usually referred to as shear dispersion or Taylor dispersion [28]. This phenomenon reduces the strength of the entropy fluctuations at a given axial location and the attenuation increases with

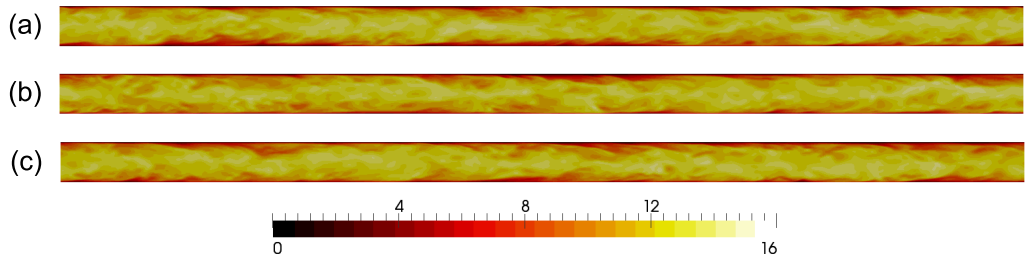

Fig. 11 Instantaneous axial velocity (m/s) at different frequencies (U_b = 10.0 m/s): (a) f=50 Hz, (b) f=100 Hz, (c) f=200 Hz.

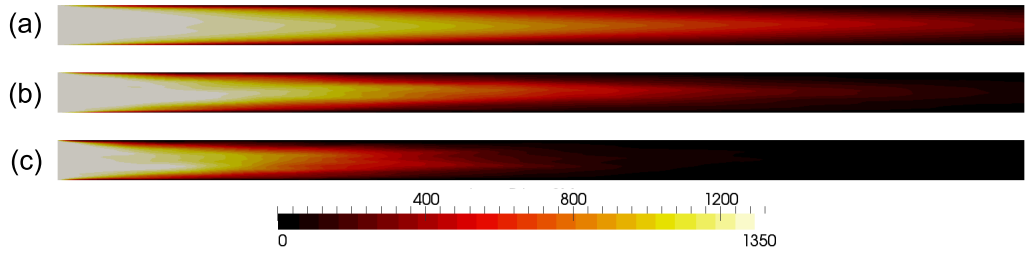

Fig. 12 Entropy variance ($J^2/(kg\ K)^2$) at different frequencies ($U_b = 10.0$ m/s): (a) f=50 Hz, (b) f=100 Hz, (c) f=200 Hz.

the axial distance. Additional contributions to the decay of entropy waves also come from the diffusion in the axial direction and turbulent mixing. Their effect is expected to increase with the residence time and with the decrease of the entropy wavelength. A smaller wavelength of the entropy perturbation leads to higher gradients making the diffusion process faster. Furthermore, as the entropy wavelength approaches the turbulent length scale, the turbulent mixing becomes more and more effective further reducing the strength of the entropy fluctuation [1, 29]. The combined effect of all these phenomena leads to the particular shape of the entropy variance shown in Fig. 12 where the entropy fluctuations in the region very close to the walls appear to decrease faster because of the lower convection velocity and therefore higher residence time and smaller wavelength.

The previous discussion suggests that the attenuation of entropy waves is strongly dependent on the velocity profile, entropy wavelength and the distance travelled by the wave (i.e. the mean residence time and its dispersion due to a non-uniform mean velocity). In order to give more insight into the dispersion phenomenon and results useful for low-order network modelling, the

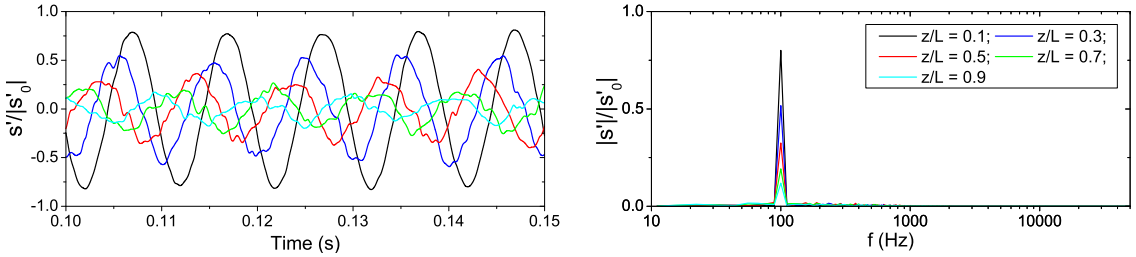

Fig. 13 Time series and frequency spectra of entropy fluctuations at different axial locations for the case $U_b = 10.0$ m/s, f=100 Hz.

instantaneous cross-section averages at different axial locations have been analysed in the frequency domain. The use of cross-section averages allows us to represent all the variables as a function of time and axial distance with results that can be directly exploited to build one-dimensional models for entropy wave propagation (the approach is similar to the one used by Morgans et al. [9]). In the following, if not differently specified, all the quantities should be interpreted as the result of the instantaneous mass flux weighted average over the cross section corresponding to each axial location.

Figure 13 shows the time series of the entropy fluctuations together with the respective frequency spectra at different locations along the axis. It is possible to note that the amplitude of the entropy waves decays on moving towards the outlet and their shape becomes more and more distorted because of the effect of both shear dispersion and turbulent fluctuations.

In order to better represent the decay of entropy waves in a form suitable for low-order modelling, it is useful to introduce an entropy transfer function, Θ, defined as the ratio between the frequency response at a given axial location (at the forcing frequency), and the entropy fluctuation at the inlet boundary:

$$\Theta(f,z) = \frac{\widehat{s}(f,z)}{\widehat{s}(f,0)} \tag{1}$$

where the circumflex indicates that the quantity should be interpreted as a complex component in the frequency domain. The entropy transfer function as defined here is a function of both the frequency and the axial location and, as every complex quantity, should be described in terms of both magnitude and phase. According to the results shown in Fig. 10, the overall decay of the

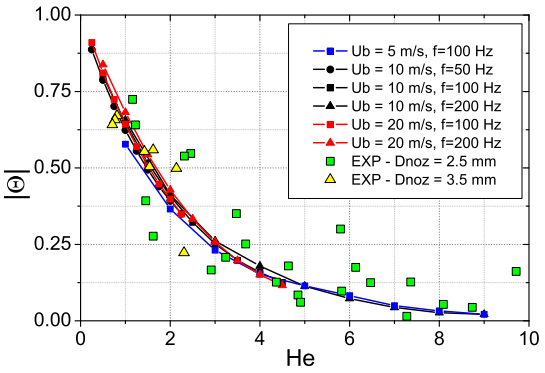

Fig. 14 Magnitude of the entropy transfer function as a function of He.

entropy fluctuations appears to be influenced by both the wavelength of the entropy fluctuation and the axial distance (or equivalently the frequency and the mean residence time of the fluctuations). These two quantities can be combined by introducing a local Helmholtz number, He, which allows us to further reduce the dimension of the problem:

$$He = \frac{f}{U_b} z \tag{2}$$

where z is the axial distance from the inlet and U_b/f represents the mean wavelength of the entropy fluctuation (the inlet bulk velocity was used as reference value). Figure 14 shows the amplitude of the entropy transfer function as a function of the local Helmholtz number. Cases with different bulk velocity were considered. The decay of entropy waves scales reasonably well with He, even if some deviations appear. These are probably due to the different shape of the velocity profile in the radial direction, which affects the differential time delay of the entropy wave across the section and therefore its dispersion, with further contributions due to turbulent mixing and diffusion which, as previously discussed, may have an important effect on the attenuation of entropy waves especially in the cases with shorter wavelength. It is also important to point out that the shape of the entropy transfer function found in the present numerical investigation and shown in Fig. 14 is in good agreement with the recent findings of Morgans et al. [9] based on DNS simulations of a simplified turbulent channel flow between two parallel plates.

A similar reduction was also performed for the experimental data and results are included in Fig. 14. Values at T1 were taken as reference, and the attenuation of entropy waves from T1

to T2 was computed. The experimental entropy transfer function was directly computed from temperature measurements, which gave results almost identical to the ones obtained by estimating the entropy at the two axial locations using the method discussed for Fig. 5. Measurements from a wide range of experiments conducted at different flow velocities were considered to demonstrate the collapse of data from high amplitude at low He exponentially decaying to low amplitudes at high He. Numerical results agree reasonably well with the experiment. Higher deviations can be observed at high He where, however, experimental results are affected by bigger uncertainties due to the smaller amplitude of high frequency harmonics. Furthermore, it should be noted that in the experiment the generation and propagation of entropy waves can be affected by some complex phenomena not included in simulations (e.g. fuel ignition and mixing) and that the single point measurement technique used in the experiments could lead to further deviations, even if comparisons with numerical results based on single point samples along the duct axis (not shown here) exhibit a similar kind of agreement. It should also be noted that in the experiment the fluctuations at the reference location (T1) are likely to be non-homogeneous over the cross section, different from the numerical simulations where a uniform profile was imposed, and for low values of He the amplitude of the fluctuations can reach the 10% of the mean value possibly generating further scattering due to non-linear behaviour. In addition, the choice of the experimental reference location is quite arbitrary and it could have an influence on the dispersion of the data (even if the trend is not affected). This point will be further discussed in Section IV B. Therefore, experimental results should be mainly used to evaluate the trend of the decay of the entropy fluctuations and from this point of view the comparison with the numerical results shows a reasonable agreement.

IV. Low-order modelling

Because of the very low computational cost, low order acoustic network codes are widely used as a preliminary design tool in the thermoacoustic analysis of real systems. Therefore it is of great interest to develop further these codes by including a more accurate and realistic description of the decay of entropy waves. As already observed, although the importance of phenomena related to the dispersion and diffusion of entropy waves has been pointed out by many authors, in low-order codes

the propagation of entropy waves is usually modelled in a very simplistic way. Stow and Dowling [30] studied the behaviour of a gas turbine combustor model in the two extreme cases of entropy waves convected without attenuation and entropy perturbations completely diffused, highlighting that the presence of entropy waves can have an important role in the stability of the system. The analysis performed in this work shows that these approximations can be a good representation of the physical behavior of the entropy transport only in the limiting cases of very small and very high He, respectively. The first attempt of introducing a more comprehensive description of the entropy wave dispersion valid in the whole range of He is probably represented by the theoretical work by Sattelmayer [7]. Over the last years, this formulation has been exploited by many other authors (e.g. [17, 31]), however, to the authors' knowledge, a direct and complete validation or assessment has never been done. Only very recently, Morgans et al. [9] attempted a more detailed analysis of the entropy convection using DNS, leading to the development of a Gaussian model for the entropy wave dispersion. Comparisons against DNS data showed that the Gaussian model was able to improve the prediction of the magnitude of the entropy transfer function compared to the Sattelmayer model. However, the assessment was limited to the magnitude of the entropy waves whereas no comparison for the phase was provided.

Experimental and numerical results obtained in the present work can be used to assess and calibrate models suitable for low-order acoustic network codes. In the following, a new theoretical model for the dispersion of entropy waves is proposed. This model only requires the mean velocity field as an input which can be easily obtained with straightforward simulations based on the RANS approach (or analytical solutions in the case of very simple flows).

A. Theoretical model for the entropy transfer function

Starting from the relation $Ds/Dt = 0$, a theoretical model for the computation of the entropy transfer function can be derived. This model is based on the convection of entropy fluctuations and considers only the differential time delay due to a non-uniform velocity profile across the radius whereas the effects of turbulent mixing and diffusion are neglected. This assumption allows us to derive a simple model and its validity over the whole range of He will be assessed a posteriori by

comparisons with the present numerical results. In the following, mean quantities will be denoted with a bar whereas the prime symbol will be used to indicate perturbations from the mean value. Furthermore, the symbols z, r, θ will be used to indicate respectively the axial, radial and tangential coordinates/components of the velocity vector. Assuming that (a) the mean flow is axial and fully developed, $\overline{\mathbf{u}} = (\overline{u}_z,\, \overline{u}_r,\, \overline{u}_\theta) = (\overline{u}_z(r),\, 0,\, 0)$; (b) the mean entropy varies only with the radius, $\overline{s}(r)$; (c) perturbations are linear and $u'_r = 0$ (u' is a function of z and θ only), the previous relation can be written as:

$$\frac{\partial s'}{\partial t} + \overline{u}_z(r)\frac{\partial s'}{\partial z} = 0 \tag{3}$$

Considering entropy fluctuations of the form $s'(z,r,t) = \widehat{s}(z,r)\exp(i\omega t)$ and a uniform entropy fluctuation at the inlet section (i.e. $\widehat{s}(0,r) = \widehat{s}_0$, as in the CFD simulations performed in this work), Eq. 3 assumes the following form:

$$\widehat{s}(z,r) = \widehat{s}_0 \exp[-i\omega z/\overline{u}_z(r)] \tag{4}$$

Finally, performing the mass-weighted average in the duct of radius R, it is possible to express the entropy fluctuation at a given axial location as:

$$\widehat{s}(z) = \widehat{s}_0 \frac{\int_0^R \overline{\rho} 2\pi r \overline{u}_z(r) \exp[-i\omega z/\overline{u}_z(r)] dr}{\int_0^R \overline{\rho} 2\pi r \overline{u}_z(r) dr} \tag{5}$$

resulting in the following expression for the entropy transfer function:

$$\Theta = \frac{\widehat{s}(z)}{\widehat{s}_0} = \frac{2}{R^2 U_b} \int_0^R r \overline{u}_z(r) \exp[-i\omega z/\overline{u}_z(r)] dr \tag{6}$$

Introducing the Helmholtz number defined in this work (see Eq. 2), Eq. 6 becomes:

$$\Theta = \frac{\widehat{s}(z)}{\widehat{s}_0} = \frac{2}{R^2 U_b} \int_0^R r \overline{u}_z(r) \exp[-2i\pi He U_b/\overline{u}_z(r)] dr \tag{7}$$

The values of the entropy transfer function of Eq. 7 can be numerically calculated using the mean velocity profile coming from numerical simulations. Results for the three different bulk velocities considered in this work are shown in Fig. 15 and compared with both numerical and experimental results. The magnitude and the phase predicted by the model are in very good agreement with results obtained in the experimental and numerical investigations, especially for $He < 3.0$. The deviation between the magnitude predicted by the model and the LES results increases with He.

This can be related to the effect of turbulent mixing and diffusion which become more and more important as the He is increased. The LES results consider all these effects and, consistently, the magnitude of the entropy transfer function predicted by the numerical simulations is always lower than the respective values determined by the low-order model.

Since the theoretical model considers only the contribution due to the differential convection, comparisons with the LES results also allow us to identify the main contributions to the decay of entropy waves as a function of He. For low values of He (small mean residence time or long wavelength of the entropy fluctuations), the magnitude of the entropy transfer function predicted by the theoretical model is very close to the LES results, therefore the main contribution to the decay of entropy fluctuations is the one coming from the different time delays determined by a non-uniform velocity profile. At high He, where the deviation between the theoretical model and the LES prediction is bigger, also the turbulent mixing and diffusion may give an important contribution to the attenuation of entropy waves. High values of He correspond to high mean residence times or short wavelengths which, as already discussed, make the diffusion and turbulent mixing processes more effective. As far as the phase is concerned, the theoretical model is in very good agreement with the LES simulations in the whole range of He investigated here suggesting that the phase of the entropy transfer function is mainly influenced by the convection of the perturbations with negligible contributions from diffusion and turbulent mixing.

It is important to point out that in typical gas turbine applications, entropy fluctuations of interest for combustion noise or thermoacoustic instability are usually characterized by low values of the Helmholtz number, typically $He < 3.0$, a range where the present formulation seems to give a good estimation of the entropy transfer function.

It is also useful to define a non-dimensional radius and a non-dimensional mean axial velocity as $\widetilde{r} = r/R$ and $\widetilde{u}_z = \overline{u}_z/U_b$ respectively. Introducing these scaled quantities into Eq. 7, a useful expression for the theoretical model can be found, allowing us to further analyse the convection of entropy fluctuations:

$$\Theta = \frac{\widehat{s}(z)}{\widehat{s}_0} = 2\int_0^1 \widetilde{r}\widetilde{u}_z(\widetilde{r})\exp[-2i\pi He/\widetilde{u}_z(\widetilde{r})]d\widetilde{r} \tag{8}$$

According to the form introduced in Eq. 8, the entropy transfer function depends only on two

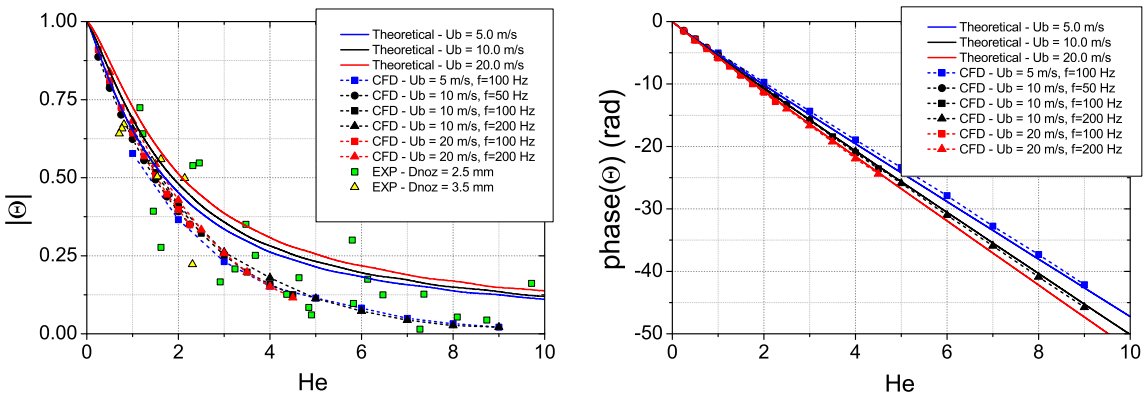

(a) Magnitude

(b) Unwrapped phase

Fig. 15 Comparison between the theoretical model and experimental and numerical results in terms of magnitude and phase of the entropy transfer function.

parameters, the Helmholtz number and the shape of the mean velocity profile through the non-dimensional function $\overline{u}_z(r/R)/U_b = \widetilde{u}_z(\widetilde{r})$. Cases with the same velocity profile are characterized by the same entropy transfer function when expressed as a function of He. Results shown in Fig. 15 were obtained using the mean velocity profile from the LES computation. Therefore, the differences between the cases characterized by different bulk velocity can be ascribed only to different shapes of the mean velocity profile. In order to have a sensitivity to the effect of the velocity profile on the shape of the entropy transfer function, it could be instructive to analyse the behaviour of the model when different functions $\widetilde{u}_z(\widetilde{r})$ are introduced. Figure 16 shows the results of such an analysis considering three different shapes of the velocity profile [32]. The first one is a parabolic laminar flow, $\widetilde{u}_z(\widetilde{r}) = 2(1-\widetilde{r}^2)$, whereas the other two cases represent fully developed turbulent flows, $\widetilde{u}_z(\widetilde{r}) = C(1-\widetilde{r})^{(1/n)}$, for different values of the exponent n (C is a constant which depends only on the value of n). Variations of the shape of the mean velocity profile introduce a non-negligible dispersion in both the magnitude and the phase of the entropy transfer function. A reliable estimation of the velocity profile is therefore mandatory for an accurate evaluation of the attenuation of entropy waves. However, it should be noted that, especially in cases characterized by a fully developed turbulent velocity profile, the trend of the entropy transfer function is dominated by the Helmholtz number and therefore also in cases where the shape of the velocity profile is affected by some uncertainties the only knowledge of He allows a reliable estimation of the decay

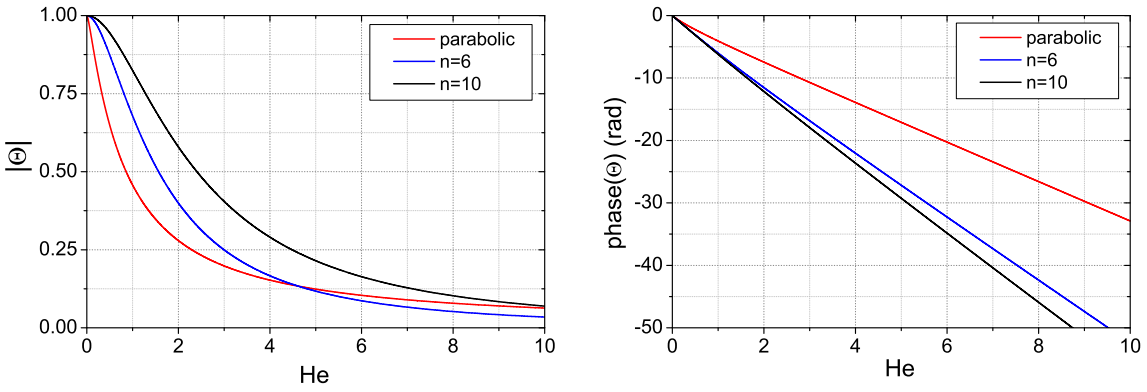

(a) Magnitude

(b) Unwrapped phase

Fig. 16 Analysis of the sensitivity of the theoretical model to the shape of the velocity profile.

of entropy waves.

In order to demonstrate the improvements that can be obtained with the proposed formulation, it could be useful to compare the experimental and numerical results with the other formulations available in the literature, namely the Sattelmayer model [7] and the Gaussian model recently proposed by Morgans et al. [9]. As the model introduced in this work, the theoretical entropy transfer function developed by Sattelmayer [7] considers only the dispersion due to the convection with a non-uniform mean velocity profile. Considering a rectangular distribution of the residence time, the entropy transfer function between the inlet and outlet sections of a duct can be written in the following form [31]:

$$\Theta = \exp(-i\omega\tau)\frac{\sin(\omega\Delta\tau)}{\omega\Delta\tau} = \exp(-i\omega\tau)\frac{\sin(\omega K\tau)}{\omega K\tau} \tag{9}$$

where τ is the mean time delay of the entropy wave from the inlet to the outlet, ω is the angular frequency of the perturbation and $\Delta\tau$ is the time spread assumed to be proportional to the time delay through a real constant K (i.e. $\Delta\tau = K\tau$). In this form, the dispersion parameter K represents the effect of the shape of the mean velocity profile (different shapes give a different non-dimensional spread, $\Delta\tau/\tau$, of the time delay). If the mean time delay is considered equal to $\tau = z/U_b$ [31], the previous expression can be written in terms of the local Helmholtz number introduced in this work, allowing a direct comparison with the present results:

$$\Theta = \exp(-2i\pi He)\frac{\sin(2\pi KHe)}{2\pi KHe} \tag{10}$$

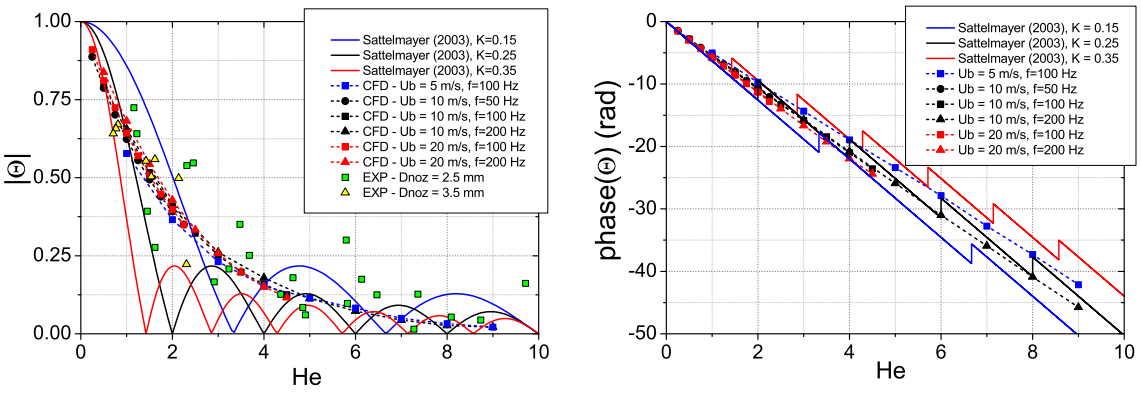

(a) Magnitude

(b) Unwrapped phase

Fig. 17 Comparison between the Sattelmayer model [7] and experimental and numerical results in terms of magnitude and phase of the entropy transfer function.

First of all, it should be noted that, similar to the model proposed in this work, the Sattelmayer model expressed as in Eq. 10 depends only on He and the shape of the velocity profile through the parameter K. Comparisons with the current experimental and numerical results are presented in Fig. 17 for several values of K. Values in the range 0.15-0.25, which is consistent with the actual velocity profiles, seem to give a reasonable estimation of both the magnitude and the phase of the entropy transfer function even if it is evident that this formulation is less accurate than the proposed model.

The model proposed by Morgans et al. [9], developed in the context of a channel flow between two parallel plates, is applied here to a duct flow. The model describes the variation of the magnitude of the entropy transfer function through a Gaussian model whereas the phase shift is simply introduced by means of a time-lag model based on the time delay of the peak of the Gaussian pulse. In the absence of a general expression that gives an estimation of the time delay associated with the convection of the Gaussian pulse at each axial location as a function of the flow basic quantities (e.g. bulk velocity), following a common practice in low-order acoustic network codes [1, 30], the time delay was computed here from the flow bulk velocity. This will also allow us to assess the reliability of this modelling assumption. Introducing again the Helmholtz number as defined in this

work, the formulation can be written as:

$$\Theta = \exp[-\omega^2/(4\pi A_{IR}^2)]\exp(-i\omega\tau) = \exp[-\pi(HeU_b/zA_{IR})^2]\exp(-2i\pi He) \tag{11}$$

where A_{IR} is a model parameter that can be found from a Gaussian model of the amplitude of the impulse response, determined for example from the probability density function of the residence time [9]. It should be noted that the parameter A_{IR} depends on the axial location as well as the bulk velocity of the flow. Exploiting the results obtained in the present work where the amplitude of the entropy transfer function has been found to scale quite well with the local Helmholtz number, the Gaussian formulation can be re-written as:

$$\Theta = \exp[-(He/A)^2]\exp(-2i\pi He) \tag{12}$$

where A is now a parameter that depends only on the shape of the mean velocity profile (in the case of entropy attenuation dominated by the shear dispersion), but not on the axial location and bulk velocity of the flow so that this formulation in only a function of He and the time delay dispersion as in the models previously discussed. Figure 18 shows comparisons between this model and the present experimental and CFD results. Values of A able to give a good fit of the magnitude of the entropy transfer function lie in the range 1.0-3.0. It should be noted that although the magnitude of the entropy transfer function is reasonably well predicted, the phase is not well represented demonstrating that the simple time-lag model based on flow bulk velocity is not able to correctly represent the phase shift when a non-uniform mean velocity profile is present. A better estimation of the time delay, for example deduced from the probability density function of the time delay as suggested by Morgans et al. [9], is therefore necessary to improve the prediction of the phase.

The analysis performed so far was based on the use of a mass-weighted average. Sometimes, as in the work by Morgans et al. [9], an area average may be preferred and therefore it is also instructive to show the behaviour of the model in the case an area-based average is used to compute average values in the duct cross section. In this case, the model of Eq. 7 can be rearranged as:

$$\Theta = \frac{\widehat{s}(z)}{\widehat{s}_0} = \frac{2}{R^2}\int_0^R r\exp[-2i\pi HeU_b/\overline{u}_z(r)]dr \tag{13}$$

Introducing the non-dimensional radius and mean axial velocity ($\widetilde{r}$ and $\widetilde{u}_z$ previously defined), Eq. 13

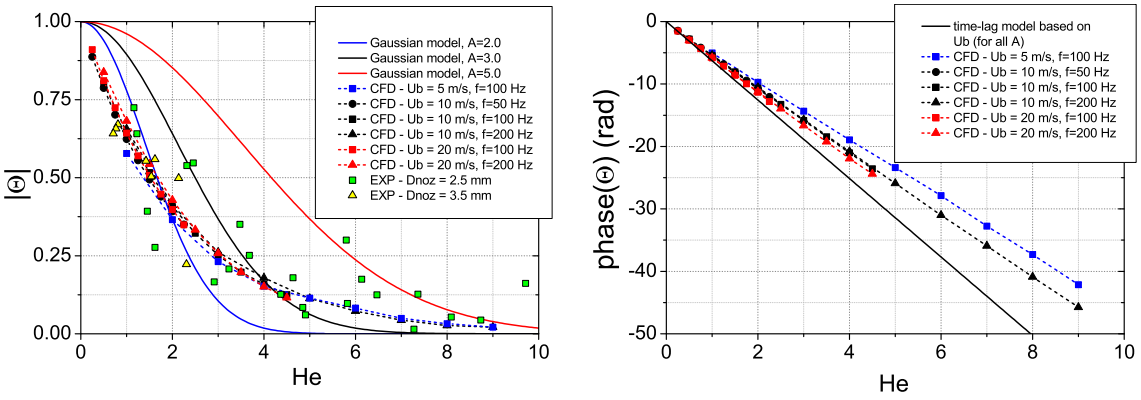

(a) Magnitude

(b) Unwrapped phase

Fig. 18 Comparison between the Gaussian model [9] (with time-lag model based on the flow bulk velocity) and experimental and numerical results in terms of magnitude and phase of the entropy transfer function.

becomes:

$$\Theta = \frac{\widehat{s}(z)}{\widehat{s}_0} = 2\int_0^1 \widetilde{r}\exp[-2i\pi He/\widetilde{u}_z(\widetilde{r})]d\widetilde{r} \tag{14}$$

Figure 19 shows comparison between the theoretical model and the CFD results based on area averages. The magnitude of the entropy transfer function is smaller compared to the previous cases because of the higher influence exerted by the flow close to the wall (characterized by a large area but a small mass flow rate), where the level of fluctuations is low as clearly shown in Fig. 12, whereas no significant differences can be observed for the phase. Also in this case, the theoretical model is in good agreement with numerical results demonstrating that the proposed approach is able to give a reliable representation of the attenuation of entropy waves also when different averaging operators are used to reduce the fluctuations to a one-dimensional form. Again, some discrepancies arise at high values of He where the same considerations reported in the discussion of Fig. 15 still apply.

B. Simplified analytical model

The theoretical model discussed in Section IV A only requires the knowledge of the mean velocity profile and can be, in principle, applied to any configuration without requiring calibration of model parameters. However, sometimes the mean velocity profile might not be available and therefore

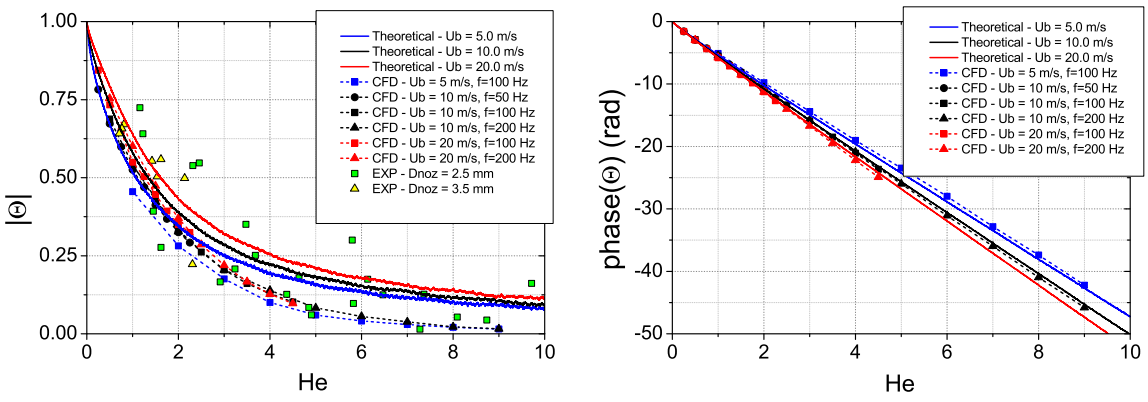

(a) Magnitude

(b) Unwrapped phase

Fig. 19 Comparison between the theoretical model and experimental and numerical results in terms of magnitude and phase of the entropy transfer function based on area average.

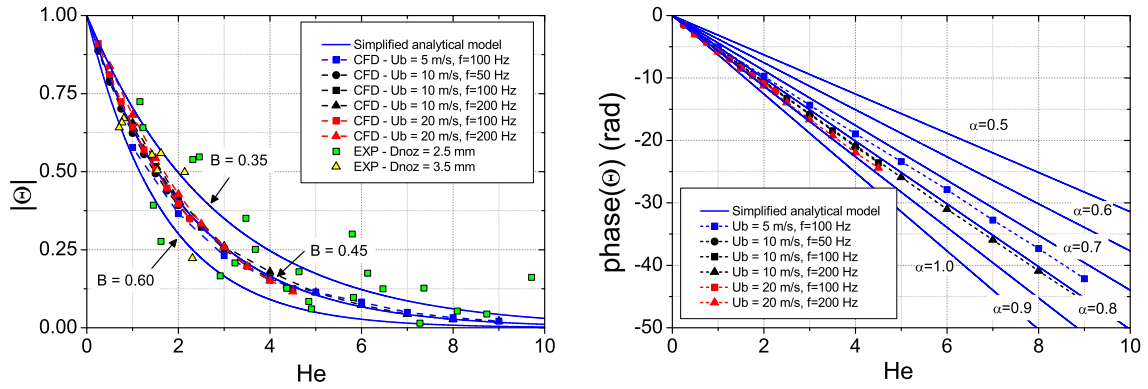

Fig. 20 Comparison between the expression in Eq. 15 and experimental and numerical results for different values of α and B.

it could also be of interest to introduce an analytical expression for the entropy transfer function. Here, the following simplified expression is proposed (valid for positive frequencies):

$$\Theta^a = \exp[-(2i\pi\alpha + B)He] \tag{15}$$

where α and B are real constants which regulate the phase shift (introducing a correction to the simple time-lag model) and the attenuation, respectively. Figure 20 shows comparisons between this formulation and both experimental and numerical results for different values of α and B. It is possible to note that a proper choice of such parameters allows a good representation of both the magnitude and the phase of the entropy transfer function found in the present investigation. The

use of this simple expression also allows us to easily describe the entropy dispersion and diffusion as a composition of subsequent steps. Let us consider for example three generic axial locations, z_0, z_1, and z_2 such that $z_0 < z_1 < z_2$, taking the first one as the reference location for the computation of the entropy attenuation. The entropy transfer function between z_0 and z_2 can be written as the product of the two intermediate transfer functions:

$$\begin{aligned}\Theta^a_{z_2-z_0} &= \frac{\widehat{s}(z_2)}{\widehat{s}(z_0)} = \Theta^a_{z_2-z_1}\Theta^a_{z_1-z_0} = \frac{\widehat{s}(z_2)}{\widehat{s}(z_1)}\frac{\widehat{s}(z_1)}{\widehat{s}(z_0)} \\ &= \exp[-(2i\pi\alpha + B)f(z_2 - z_1)/U_b]\exp[-(2i\pi\alpha + B)f(z_1 - z_0)/U_b] \\ &= \exp[-(2i\pi\alpha + B)f(z_2 - z_0)/U_b]\end{aligned} \tag{16}$$

This clearly shows that if the decay of entropy waves follows an exact exponential form, the shape of the entropy transfer function is independent of the reference location used to compute the relative decay (this is in general not true for the other models where the decay of the entropy fluctuations also depends on the previous history). Since, as shown in Fig. 20, the exponential model is a good approximation of the data found in the CFD investigation, this partly justifies the use in the experiments of an arbitrary reference plane for the data reduction making the experimental transfer function meaningful and consistent at least for getting the trend of the decay of entropy fluctuations. From another perspective, the good agreement between experiments and numerical results can be also considered an indirect assessment of the exponential-like behaviour of the attenuation of entropy waves.

V. Conclusions

The propagation of entropy waves in a small scale rig has been investigated using both experiments and numerical simulations. Results show that the amplitude of entropy waves decays as a function of the frequency and the mean residence time of the wave and the entropy transfer function scales well with a local Helmholtz number based on the entropy wavelength and the axial distance.

Considering the differential convection as the dominant mechanism in the decay of entropy waves, a new theoretical model for the entropy transfer function, suitable for application in low-order acoustic network codes, has been proposed. This model only requires the knowledge of the mean velocity profile which can be obtained from a quick and straightforward RANS calculation of

the mean flow. Validation against the present experimental and CFD results shows that the model is able to properly predict both the magnitude and phase of the entropy transfer function, especially in the intermediate and low range of the Helmholtz number.

Comparisons between the proposed formulation and numerical results highlight the important role exerted by the shear dispersion arising from spatial variations of the mean velocity profile in the attenuation of entropy fluctuations for low values of the Helmholtz number. For high values of the Helmholtz number results suggest that also the turbulent mixing and diffusion could give an important contribution to the overall decay of the entropy fluctuation.

According to the developed theoretical model, the shear dispersion arising from the differential convection is regulated by only two parameters, the local Helmholtz number introduced in this work and the shape of the velocity profile with the former that plays the most important role in determining the decay of the entropy transfer function, especially in the case of fully developed turbulent flows. Therefore, also in cases where an accurate evaluation of the shape of the mean velocity profile is not available, the knowledge of the Helmholtz number allows a reliable estimation of both the magnitude and the phase of the entropy transfer function.

It is important to point out that both the range of velocities and the geometry investigated in this work can be far from real engine applications. Therefore, further investigations should be carried out in the future in configurations much closer to real engines usually characterized by complex flow structures such as recirculation zones induced by swirling air flows which make the convection and mixing processes a completely three dimensional phenomenon. Furthermore, in this investigation the diameter of the duct was kept constant. However, the duct diameter limits the turbulence length scale and this may have an effect on the interaction between the entropy wave and the turbulence suggesting that the decay of entropy waves can also be a function of a Helmholtz number based on the entropy wavelength and duct radius. This should be addressed in future work together with an analysis of the behaviour of entropy diffusion and dispersion in the case of high amplitude of the fluctuations where a higher impact of the temperature oscillations on the flow field may be expected.

Acknowledgments

The research leading to these results has received funding from the European Community's Seventh Framework Programme (FP7/2007-2013) under Grant Agreement n. 265586 and was conducted within the IMPACT-AE (Intelligent Design Methodologies for Low Pollutant Combustors for Aero-Engines) project.

References

[1] Dowling, A. P. and Mahmoudi, Y., "Combustion noise," *Proceedings of the Combustion Institute*, Vol. 35, No. 1, 2015, pp. 65 – 100.

[2] Marble, F. and Candel, S., "Acoustic disturbance from gas non-uniformities convected through a nozzle," *Journal of Sound and Vibration*, Vol. 55, No. 2, 1977, pp. 225 – 243.

[3] Motheau, E., Mery, Y., Nicoud, F., and Poinsot, T., "Analysis and Modeling of Entropy Modes in a Realistic Aeronautical Gas Turbine," *ASME. J. Eng. Gas Turbines Power*, Vol. 135, No. 9.

[4] Hochgreb, S., Dennis, D., Ayranci, I., Bainbridge, W., and Cant, S., "Forced and self-excited instabilities from lean premixed, liquid-fuelled aeroengine injectors at high pressures and temperatures," *Proc. ASME Turbo Expo*. GT2013-95311.

[5] Motheau, E., Nicoud, F., and Poinsot, T., "Mixed acoustic-entropy combustion instabilities in gas turbines," *Journal of Fluid Mechanics*, Vol. 749, 2014, pp. 542–576.

[6] Dowling, A. P. and Hubbard, S., "Instability in lean premixed combustors," *Proceedings of the Institution of Mechanical Engineers, Part A: Journal of Power and Energy*, Vol. 214, No. 4, 2000, pp. 317 – 322.

[7] Sattelmayer, T., "Influence of the Combustor Aerodynamics on Combustion Instabilities from Equivalence Ratio Fluctuations," *J. Eng. Gas Turbines Power*, Vol. 125, 2003, pp. 11 – 19.

[8] Huet, M. and Giauque, A., "A nonlinear model for indirect combustion noise through a compact nozzle," *Journal of Fluid Mechanics*, Vol. 733, 2013, pp. 268–301.

[9] Morgans, A. S., Goh, C. S., and Dahan, J. A., "The dissipation and shear dispersion of entropy waves in combustor thermoacoustics," *Journal of Fluid Mechanics*, Vol. 733, R2.

[10] M. Muthukrishnan, W. C. S. and Neale, D. H., "Separation of Hydrodynamic, Entropy, and Combustion Noise in a Gas Turbine Combustor," *AIAA Journal*, Vol. 16, No. 4, 1978, pp. 320–327.

[11] Zukoski, E. E. and Auerbach, J. M., "Experiments concerning the response of supersonic nozzles to fluctuating inlet conditions," *Journal of Engineering for Power*, Vol. 98, No. 1, 1976, pp. 60–64.

[12] Bake, F., Richter, C., Mühlbauer, B., Kings, N., Röhle, I., Thiele, F., and Noll, B., "The Entropy Wave

Generator (EWG): A reference case on entropy noise," *Journal of Sound and Vibration*, Vol. 326, No. 3-5, 2009, pp. 574 – 598.

[13] Bake, Kings, Fischer, and Röhle, "Experimental investigation of the entropy noise mechanism in aero-engines," *International Journal of Aeroacoustics*, Vol. 8, No. 1, 2009, pp. 125–141.

[14] Dowling, A. P. and Stow, S. R., "Acoustic Analysis of Gas Turbine Combustors," *Journal of Propulsion and Power*, Vol. 19, No. 5, 2003, pp. 751 – 764.

[15] Goh, C. S. and Morgans, A. S., "Phase prediction of the response of choked nozzles to entropy and acoustic disturbances," *Journal of Sound and Vibration*, Vol. 330, No. 21, 2011, pp. 5184 – 5198.

[16] Duran, I. and Moreau, S., "Solution of the quasi-one-dimensional linearized Euler equations using flow invariants and the Magnus expansion," *Journal of Fluid Mechanics*, Vol. 723, 2013, pp. 190–231.

[17] Goh, C. S. and Morgans, A. S., "The Influence of Entropy Waves on the Thermoacoustic Stability of a Model Combustor," *Combustion Science and Technology*, Vol. 185, No. 2, 2013, pp. 249–268.

[18] Ballantyne, A. and Moss, J. B., "Fine Wire Thermocouple Measurements of Fluctuating Temperature," *Combustion Science and Technology*, Vol. 17, No. 1-2, 1977, pp. 63–72.

[19] McAdams, W. H., *Heat Transmission*, McGraw Hill, New York, 3rd ed., 1954.

[20] Shapland, T., Snyder, R., U, K. P., and McElrone, A., "Thermocouple frequency response compensation leads to convergence of the surface renewal alpha calibration," *Agricultural and Forest Meteorology*, Vol. 189-190, 2014, pp. 36 – 47.

[21] Weller, H. G., Tabor, G., Jasak, H., and Fureby, C., "A tensorial approach to computational continuum mechanics using object-oriented techniques," *Computers in Physics*, Vol. 12, No. 6.

[22] Ferziger, J. H. and Peric, M., *Computational Methods for Fluid Dynamics*, Springer-Verlag Berlin Heidelberg, 3rd ed., 2002.

[23] Tabor, G. and Baba-Ahmadi, M., "Inlet conditions for large eddy simulation: A review," *Computers & Fluids*, Vol. 39, No. 4, 2010, pp. 553 – 567.

[24] Orlanski, I., "A simple boundary condition for unbounded hyperbolic flows," *Journal of Computational Physics*, Vol. 21, No. 3, 1976, pp. 251 – 269.

[25] van Driest, E. R., "On Turbulent Flow Near a Wall," *Journal of the Aeronautical Sciences*, Vol. 23, No. 11, 1956, pp. 1007 – 1011.

[26] Pope, S. B., *Turbulent Flows*, Cambridge University Press, 2000.

[27] Eggels, G., Unger, F., Weiss, M., Westerweel, J., Adrian, R., Friedrich, R., and Nieuwstadt, F., "Fully developed turbulent pipe flow: a comparison between direct numerical simulation and experiment," *J. Fluid Mechanics*, Vol. 268, 1994, pp. 175–209.

[28] Taylor, G., "Dispersion of Soluble Matter in Solvent Flowing Slowly through a Tube," *Proceedings of the Royal Society of London A: Mathematical, Physical and Engineering Sciences*, Vol. 219, No. 1137, 1953, pp. 186–203.

[29] Taylor, G., "The Dispersion of Matter in Turbulent Flow through a Pipe," *Proceedings of the Royal Society of London A: Mathematical, Physical and Engineering Sciences*, Vol. 223, No. 1155, 1954, pp. 446–468.

[30] Stow, S. R. and Dowling, A. P., "Thermoacoustic oscillations in an annular combustor," *Proceedings of the ASME Turbo Expo*. 2001-GT-0037.

[31] Eckstein, J. and Sattelmayer, T., "Low-Order Modeling of Low-Frequency Combustion Instabilities in Aeroengines," *Journal of Propulsion and Power*, Vol. 22, No. 2, 2006, pp. 425 – 432.

[32] White, F., *Fluid Mechanics*, McGraw-Hill series in mechanical engineering, McGraw Hill, 2011.